Cutting-Edge Laser Forming in High-Precision Hole Fabrication for Thin Glass Applications

Meenkyo Seo[1], Jinhong Jeun[1], Jeonghun Woo[1], Haesook Lee[1], Doowon Lee[1], Jekil Ryu[1], Seungjoo Lee[1], and Cheollae Roh[1]

[1]Mechatronics Technology Research Center, Samsung Display Co. Ltd., 1 Samsung-ro, Yongin-si, Gyeonggi-do 17113, Republic of Korea

Abstract

We demonstrate a novel laser forming technique for precise hole fabrication in thin glass substrates for camera holes on OLED displays. Using controlled heat gradients and stress dynamics, interior holes are generated within 0.5 seconds with sub-5 µm average chipping and no heat-affected zone. This high-precision process enables scalable solutions for advanced applications, such as high-resolution OLED displays, requiring small-diameter holes in thin glass with minimal thermal and structural damage.

Author Keywords

Laser glass cutting; Transparent material; Hole fabrication; Laser forming; High-precision.

1. Introduction

Precision machining of hole in thin glass substrates has become increasingly essential, as these substrates are integral to the functionalities of advanced optics, microfluidics, and display technologies [1,2]. Yet, traditional methods for hole fabrication, including mechanical drilling and chemical etching, have difficulties to achieve the required accuracy and might introduce defects such as chipping and distortion [3].

Ultrashort pulsed laser (USP) has emerged as a powerful alternative, offering exceptional flexibility and precision. Especially, previous research has demonstrated the efficacy of USP Bessel beams in producing clean, high-quality features in glass, highlighting their potential for complex applications [4]. Their stable intensity profile and non-diffracting properties allow for efficient material ablation while reducing thermal stress on surrounding areas, which is critical for maintaining the integrity of thin glass. Despite these advantages, challenges remain in fully separating the cut segments from substrates when machining interior holes, since the single-pass scribing of the Bessel beam would not generate a macroscopic kerf [5,6]. In particular, as targeted hole diameter decreases, the separation of hole segments becomes harder, often resulting in undesirable chipping due to uneven loading.

In order to address these challenges, we propose a laser-induced thermal deformation (i.e. laser forming) for clean and high-precision hole fabrication. In our approach, a picosecond laser with a Bessel beam profile creates a precise initial hole through the glass thickness. Following this, a CO_2 laser is employed to induce localized thermal distortion for reshaping the hole segment, resulting in spontaneous separation from the substrate. Such a methodology allows high-quality hole generation in thin glass even with small diameters due to the non-thermal effect of the ultrashort pulse laser and shortening of hole segment itself by laser forming.

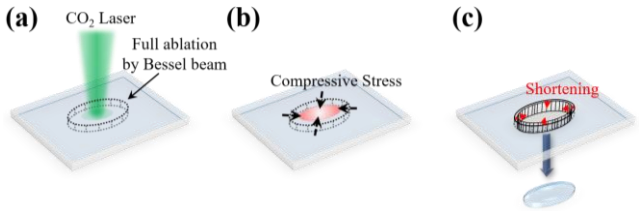

Figure 1. Schematic illustration for laser forming methodology. (a) CO_2 laser forming after full ablation via picosecond laser Bessel beam. (b) Compressive stress applied to the molten core during the cooling process. (c) Spontaneous separation due to shortening of inner hole diameter.

2. Laser Forming for Hole Fabrication in Glass

Figure 1 illustrates the laser forming methodology for precision glass processing. The full ablation with USP Bessel beam generates a precise hole in a 200 µm thick glass substrate. Note that hole segment, especially for small diameters, cannot be separated due to the constraint of closed contour geometry. To cleave the inner hole, a CO_2 laser induced thermal shaping is introduced as illustrated in Fig. 1(a). As the process transitions into the cooling phase (Figure 1(b)), the plastic compressive stress is restricted from the unheated edge, since the thermal expansion in the heated area is incapable of generating enough stress to bend the glass substrate [7]. Notably, the localized heating with the Gaussian spatial distribution induces the softening zone at the center of glass in these pre-defined regions. Such a softening area allows a high flexibility through laser forming without compromising the hole's structural integrity. Hence, the hole segment is shortens due to the accumulated stresses and differential contraction while increasing thickness of the heated area as depicted in Fig. 1(c), resulting in spontaneously clean separation.

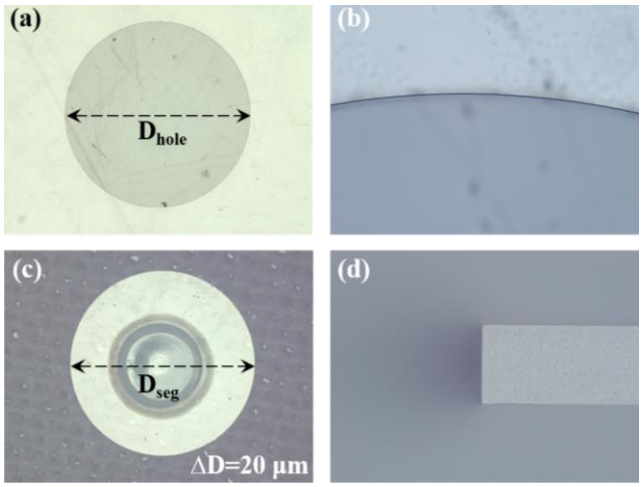

Figure 2. Characterization of hole cutting via laser forming process. (a) Optical microscope image of approximately 4.0 mm diameter hole, magnified cutting line (b), and separated hole segments (c). ΔD is the difference in diameter between hole (D_{hole}) and segment (D_{seg}). (d) Edge of hole after cleaving cross-section.

ISSN 0097-996X/25/5602-1230-$1.00 © 2025

3. High-Precision Interior Hole Cutting

Figure 2 presents the outcomes of hole cutting via the laser forming methodology, highlighting the precision and mechanical response of glass to this advanced technique. For initial condition, the full ablation was performed by a picosecond laser system delivering 3 ps laser pulses with an energy of 25 μJ at a repetition rate of 250 kHz, a center wavelength of 1035 nm, and 3 of burst mode with 0.8 μm of shot pitch and Bessel beam profile. CO_2 laser with 36 W was then applied on the center of the hole for 200 ms of exposure time. The material was transparent alkaline earth boro-aluminosilicate glass with 200 μm thickness. Clean and precise around 4.0 mm diameter hole was successfully generated within effective process time of about 0.5 s as depicted in Fig. 2(a). The high-magnification image in Fig. 2(b) further emphasizes the smooth and uniform interior surface of the hole, indicating minimal thermal damage and superior geometrical control. A noteworthy observation is depicted in Fig. 2(c), where the separated hole segment reveals a slight reduction in diameter as 20 μm. This discrepancy suggests the occurrence of material contraction during the cooling phase, likely due to the generation of compressive stresses within the molten glass. Such stresses facilitate a controlled, uniform shortening, which is consistent with the material's response to rapid thermal cycling inherent in the laser forming process. To further evaluate the quality of the cut, Figure 2(d) provides a detailed view of the hole's edge, which has been cross-sectioned through its center. The edge profile exhibits a sharp, clean boundary with a consistent 90-degree angle relative to the surface, indicative of precise energy deposition and controlled material removal. This sharp edge geometry contrasts favorably with the tapering and edge rounding often observed in traditional laser cutting techniques.

4. Mechanism of Laser Forming Process

In order to reveal the separation mechanism of the hole cutting via laser forming process, the numerical simulation was performed as depicted in the Fig. 3. Figure 3(a)-(c) present simulated thermal profiles on the surface of glass subjected to CO_2 laser irradiation with beam diameters of 0.89 mm, 1.34 mm, and 1.82 mm at the $1/e^2$ of peak intensity level, respectively, under a constant laser power of 28 W (i.e. varying the thermal gradient). To model the thermal response of boro-aluminosilicate glass, the heat transfer equation was numerically discretized using the finite difference method [8]. The governing equation for temperature evolution T(t) over time t is expressed as:

$$\frac{\partial T}{\partial t} = \alpha\left(\frac{\partial^2 T}{\partial r^2}\right) + \frac{Q(r,z,t)}{\rho c_p} \quad (1)$$

where α is the thermal diffusivity, Q(r, z, t) represents the heat source term with beam diameter d and r direction, ρ is the density, and c_p is the specific heat capacity. The heat source term Q(r, z, t) was modeled as a Gaussian distribution to reflect the intensity profile of the laser beam:

$$Q(r,z,t) = \frac{P\cdot\exp(-2r^2/(d/2)^2)}{\pi(d/2)^2}\cdot\delta(z) \quad (2)$$

where P is the laser power and d/2 is the $1/e^2$ radius of the Gaussian beam. The impulse function $\delta(z)$ is adopted, since CO_2 laser irradiation is treated as a surface heating source. The boundary condition can be expressed by:

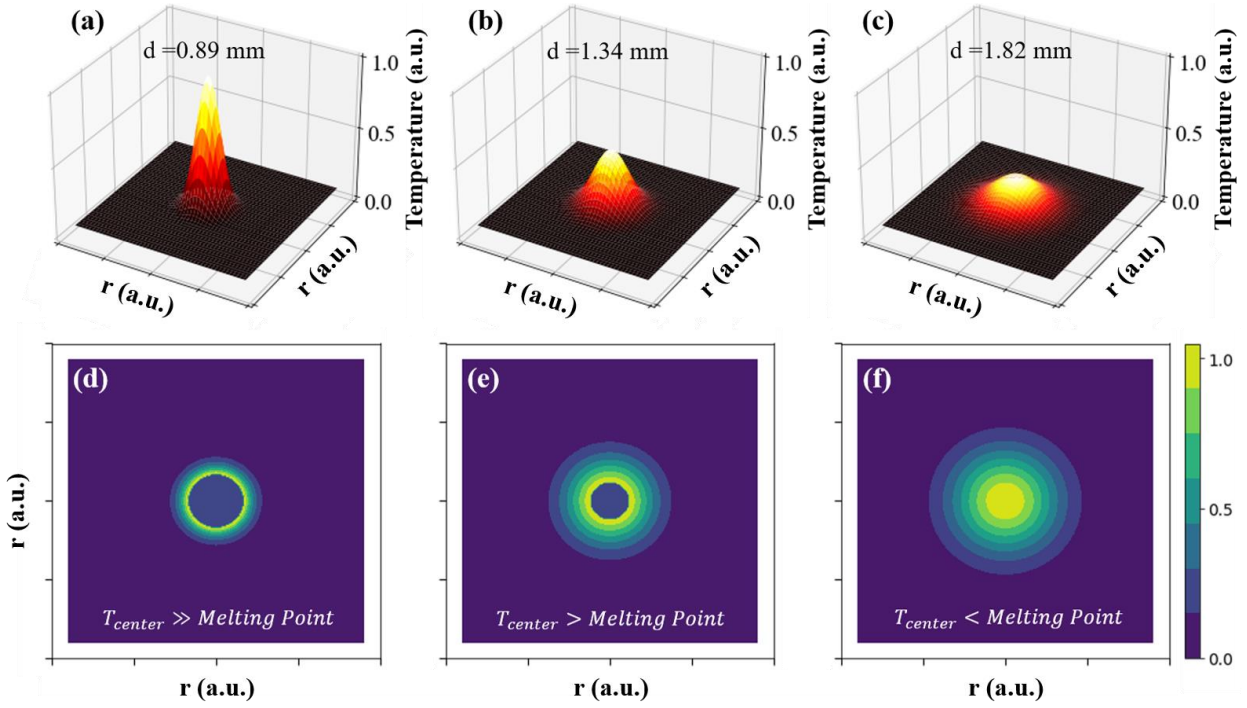

Figure 3. Numerical simulation of CO_2 laser induced thermal distribution and thermal stress on the glass. (a)-(c) Simulated thermal profile on the surface of the glass with CO_2 laser beam diameters of 0.89 mm, 1.34 mm, and 1.82 mm, respectively, under a constant laser power. The thermal profiles are normalized by a peak value of 0.89 mm case. (d)-(f) Calculated thermal stress distribution using thermal profile results corresponding to each (a)-(c).

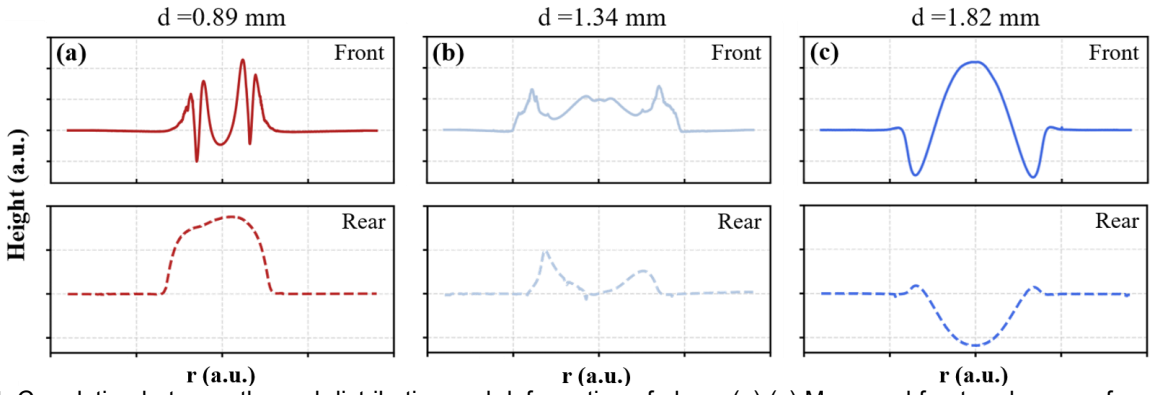

Figure 4. Correlation between thermal distribution and deformation of glass. (a)-(c) Measured front and rear surface profile of hole segments after laser forming with CO_2 laser beam diameters of 0.89 mm, 1.34 mm, and 1.82 mm, respectively, under a 28 W laser power.

$$-k\frac{\partial T}{\partial z} + h(T_s - T_0) + B\varepsilon(T_s^4 - T_0^4) = \alpha Q(r,z,t) \quad \text{at z=0} \qquad (3)$$

$$-k\frac{\partial T}{\partial n} = h(T_s - T_0) \quad \text{at z = rear surface} \qquad (4)$$

where, the direction cosine of boundary of n and the convection heat-transfer coefficient of h. Utilizing results of thermal profile, induced thermal stress (σ_{therm}) is given by [9],

$$\sigma_{therm} = \frac{E\beta\Delta T}{1-\theta} \qquad (5)$$

where θ is the Poisson's ratio, E and β are the Young's modulus and the coefficient of linear expansion, respectively. The temperature reaches the melting point of the glass (or higher), causing the material to melt. A molten pool doesn't resist deformation as much as solid glass. Thus, the material can deform freely or undergo phase changes (melting), and it doesn't contribute significantly to the thermal stress, since thermal stress is generated by differences in expansion between regions. Hence, the thermal stress over melting point is not taken into consideration.

For the 0.89 mm beam, the simulation results reveal the highest thermal gradients, with a concentration of heat at the center of the irradiated area. The temperature at the center of the glass reaches values significantly above the melting point of the alumino-borosilicate glass, while the temperature decreases rapidly toward the edges of the beam. This sharp thermal gradient generates significant thermal stress, particularly near the center of the irradiated area, where the material is most heated. The molten pool formation would be observed at the center, where the glass transitions into a molten state, resulting in lower mechanical strength and a change in material behavior compared to the surrounding solid glass. This phase transition contributes to a redistribution of the stresses, with the center experiencing compressive thermal stress while the solid edges experience tensile stress. In the case of the 1.34 mm beam, the energy distribution is more spread out, leading to lower thermal gradients compared to the 0.89 mm beam, while the temperature at the center still approaches the melting point. The temperature distribution in this case remains more uniform across the irradiated region, leading to lower thermal stresses at the center and edges. The glass undergoes less expansion at the center, and the thermal stress is more evenly distributed. The absence of significant melting reduces the magnitude of compressive and tensile stresses in the central and peripheral regions, respectively. As a result, the thermal stress distribution for the 1.34 mm beam would be less pronounced, with moderate gradients compared to the 0.89 mm case. For the 1.82 mm beam, the larger beam size results in an even more gradual temperature distribution, leading to the lowest thermal gradients among the three cases. The temperature at the center reaches only the softening point, and there is no molten pool formation. In this case, the temperature distribution is nearly uniform, resulting in minimal thermal stresses. The thermal stress remains relatively low across the entire irradiated area due to the even heating and the absence of a molten phase transition. The thermal expansion of the material is more uniform, and the overall thermal stress distribution is less severe, with the material undergoing expansion without significant constraints from the surrounding cooler material.

To verify the simulation results, the evolution of hole segment depends on thermal profile was tracked as shown in Fig. 4. For the 0.89mm case, the glass undergoes a pronounced concave deformation at the center of the beam, accompanied by an upward curvature along the edges which is consistent with simulation results. As the beam diameter increases, the thermal gradient becomes less steep, resulting in a more uniform deformation pattern as shown in Fig. 4(b) and 4(c). The 1.82 mm beam diameter, for example, produces a bi-convex lens-like shape, indicative of a more evenly distributed thermal stress across the glass surface while the intermediate state is induced for 1.34 mm beam. The simulations corroborated these experimental findings, demonstrating that deformation patterns are driven by the interplay between the Gaussian heat profile of the CO_2 laser, thermal gradients, and the material's state transitions. This deformation mechanism effectively shortens the hole segment while increasing the glass thickness at the beam's periphery, promoting the spontaneous separation of the material without the need for additional mechanical intervention.

5. Optimization for High-Quality Hole Fabrication

The interplay between thermal gradient intensity and material deformation governs the efficiency of hole segment separation due to the induction of pronounced shortening effect. For quantifying the shorten length of the hole segments as a function of thermal profiles, we investigated how the shorten length evolves by varying the beam diameters with the fixed laser power as 28 W (Figure 5(a)). A minimum hole segment diameter in laser forming occurs at a beam diameter of approximately 1.56 mm. This condition

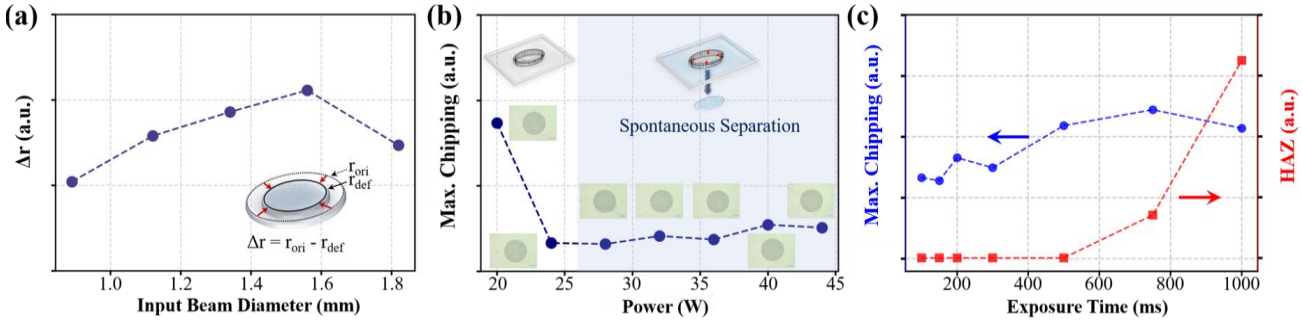

Figure 5. Optimization of laser parameters for high-quality hole cutting. (a) The relationship between thermal distribution and material contraction. The r_{ori} and r_{def} indicate original radius before thermal shaping and radius of deformed hole after CO_2 laser irradiation (inset). (b) Incident laser power and (c) exposure time dependence for chipping and thermal damage in laser forming process.

corresponds to the maximum shortening radius (Δr), signifying an optimal thermal gradient at given laser power, which facilitates more effective and controlled material separation.

The relationship between applied CO_2 laser power and the resulting chipping levels during hole segment separation is shown in Fig. 5(b), with laser power ranging from 20 W to 44 W, incremented in steps of 4 W. The experimental results reveal that at 20 W, the maximum chipping was observed, while other power levels consistently produced low chipping levels. This suggests that at 20 W, the laser power is insufficient to generate a wide enough kerf, resulting in increased material resistance and fragmentation rather than clean separation. On the other hand, beyond 24 W, the hole segments began to separate spontaneously, likely due to the more effective kerf formation as these higher power levels. Notably, across all tested power levels, no heat affected zone (HAZ) were detected as presented in inset of Fig. 5(b), affirming that the thermal impact on the glass is minimal and does not compromise its structural integrity. Additionally, a hole fabrication was performed within 0.5 seconds, achieving an average chipping size of less than 5 μm. These results, obtained with a 1.56 mm beam diameter, which produced the homogenous hear profile, highlight the efficacy across a wide power range, consistently achieving clean, spontaneous hole segment separation with minimal chipping and no HAZ. Furthermore, the impact of varying exposure times on chipping and HAZ during the CO_2 laser cutting process is investigated as shown in Fig. 5(c). The exposure times ranging from 100 ms to 750 ms result in low chipping levels, maintaining the integrity of the cut. Note that, below 100 ms, the incomplete separation was occurred due to lack of thermal energy. Conversely, at 1000 ms, the chipping level remains low, but there is a significant increase in the HAZ around the hole, indicating excessive thermal input. Such thermal impacts possess adversely affect the quality of the cut and the overall integrity of the glass. Hence, it is essential to optimize exposure time to balance the reduction of chipping with control over thermal damage for ensuring both high-quality cuts and efficient material removal. These findings substantiate the method's potential for advanced glass machining applications, where stringent tolerances and minimal thermal impact are critical.

6. Conclusion

In this study, we demonstrated a novel laser forming methodology for precision hole cutting in thin glass substrates. This approach addresses the significant challenges associated with conventional laser techniques, particularly the difficulties in separating hole segments due to small hole sizes and interior geometries, which often result in substantial chipping and distortions. The differential thermal expansion and compressive stress controlled by thermal profiles of CO_2 laser during the cooling phase play a crucial role in achieving high-quality cuts. The physical mechanism was proved by tracing the surface morphology of hole segment depends on transferred thermal distribution to glass and numerical simulation of heat profile and thermal stress on the glass. In conclusion, our laser forming methodology not only improves manufacturing efficiency but also expands the potential for high-precision applications such as OLED displays, high-resolution touch panels, and other advanced optical devices.

7. References

1. Wlodarczyk, K. L. et al., "Rapid Laser Manufacturing of Microfluidic Devices from Glass Substrates," Micromachines **9**, 409 (2018).
2. Hamed, H. et al., "Applications, materials, and fabrication of micro glass parts and devices: An overview," Mater. Today. **66**, 194-220 (2023).
3. Tsai, C. -H. & Huang, B. –W., "Diamond scribing and laser breaking for LCD glass substrates," J. Mater. Process. Technol. **198**, 350-358 (2008).
4. Vetter, C. Giust, R. Furfaro, L. Billet, C. Froehly, L. Courvoisier, F., "High Aspect Ratio Structuring of Glass with Ultrafast Bessel Beams," Materials **14**, 6749 (2021).
5. Gong, A. et al., "Theoretical modeling and experimental study in femtosecond Bessel beam ablation of α-quartz," Opt. Laser Technol. **178**, 111227 (2024).
6. Fan, X. Rong, Y. Zhang, G. Wu, C. Luo, Y. Huang, Y., "Combined laser cutting process for interior holes in thick glasses," *J. Non-Cryst. Solids* **621**, 122647 (2023).
7. Imhan, K. I., et al., "Features of laser tube bending processing based on laser forming: a review," Journal of Lasers, Optics & Photonics **5**, 1000174 (2018).
8. Tran, H. –C. Lo, Y. –L., "Heat transfer simulations of selective laser melting process based on volumetric heat source with powder size consideration," J. Mater. Process. Technol. **255**, 411-425 (2018).
9. Junke, J. & Xinbing, W., "A numerical simulation of machining glass by dual CO2-laser beams," Opt. Laser Technol. **40**, 297-301 (2008).